Available online at www.sciencedirect.com
ScienceDirect
International Journal of Heat and Mass Transfer 51 (2008) 4850–4861
International Journal of HEAT and MASS TRANSFER
www.elsevier.com/locate/ijhmt

Effect of vent aspect ratio on unsteady laminar buoyant flow through rectangular vents in large enclosures

A.K. Sleiti

Mechanical, Materials and Aerospace Engineering Department, University of Central Florida, Orlando, FL 32816, United States

Received 19 June 2007; received in revised form 21 February 2008
Available online 16 April 2008

Abstract

The effects of vent aspect ratio on oscillatory flow regime through a horizontal opening were studied numerically. The physical model consisted of a vertical rectangular enclosure divided into two chambers by a horizontal partition. The partitions contained a slot that connected the two chambers. The upper chamber contains cold air and the lower chamber contains hot air. A density differential due to the different temperatures drives the interaction between the two chambers. The opposing forces at the interface between the two chambers create a gravitationally unstable system, and an oscillating exchange of fluid develops. Results were obtained for cases with $L/D = 1$, 0.5, and 2.0, where L represents the thickness of the partition and D represents the slot width of the opening in the partition. Results indicate that the flow exchange increases with partition thickness $L/D = 0.5$ and decreases for $L/D = 2$. The frequency of the oscillatory flow pattern is also examined for the different cases. Sudden bursts of upflow with a corresponding downflow have been documented and compared with experimental observations in the literature. The time traces of velocity and temperature fields for this flow regime reveal interesting mechanisms, which have been explained.
© 2008 Elsevier Ltd. All rights reserved.

Keywords: Laminar unsteady buoyant flow; Oscillatory flow regime; Conduction flow regime

1. Introduction

The problem of natural convection heat and mass transfer has been studied extensively by many authors (see [1]). The problem of natural convection in enclosures with the top plate colder than the bottom plate has been treated extensively in the literature as well. However, the problem of heavier fluid on top of lighter fluid separated by a narrow vent has not been dealt with analytically or numerically. Such a flow configuration occurs in large ships and buildings where elevator shafts, stairwells, service shafts, etc. can act as vents connecting two floors. The flow in these vents is buoyancy-generated due to a fire in the bottom enclosure or due to leakage of contaminant gases. It is known that the worst killer in fires is the smoke inhalation because of the toxic gaseous species. In a context of worldwide concern about fire safety, engineers pay more and more attention to the smoke management in buildings. When focusing on how to conserve safety in buildings during a fire catastrophe, the first thing that comes to mind is to evacuate the smoke and heat released by the fire; therefore research is being done on optimization of the smoke evacuation design. Predicting the smoke characteristics in a building subject to a fire are depends on the geometry of the fire compartment, type of fire, the ambient conditions outside the buildings, etc. [2]. A literature review in numerical modeling of movement and behavior of smoke produced from fires in tunnels can be found in Kashef et al. [3]. The transient flow of gases may have several modes and the heat transfer mechanism is of interest especially when the flow becomes oscillatory. Early studies of flow through apertures connecting two enclosures were limited to openings in vertical partitions. The fundamental deference between flow through a vent in vertical partition and the flow through a horizontal partition is the stable

E-mail address: asleiti@mail.ucf.edu

0017-9310/$ - see front matter © 2008 Elsevier Ltd. All rights reserved.
doi:10.1016/j.ijheatmasstransfer.2008.02.027

Nomenclature

D	width of the vent
g	acceleration due to gravity
$H1$	width of the enclosure
$H2$	height of the enclosure
L	height of the vent
L/D	vent aspect ratio
Nu	Nusselt number
p	total pressure less the hydrostatic pressure
P	dimensionless pressure $= p/(\rho\alpha^2/L^2)$.
Pr	Prandtl number
Ra	Rayleigh number $= g\beta\Delta TL^3/v\alpha$
Ra_{critical}	critical value of Ra for onset of flow through the vent
Re_Δ	densimetric Reynolds number $= V_\Delta H/v$
t	time
t_c	time constant
T	temperature
T_{cold}, T_c	initial temperature of fluid in upper chamber
T_{hot}	initial temperature of fluid in lower chamber
T_{ref}	reference temperature
ΔT_i	initial temperature difference between upper and lower chamber
u,v	components of velocity in x and y directions, respectively
U,V	dimensionless components of velocity in x and y directions, respectively
x,y	horizontal and vertical coordinates
X,Y	dimensionless horizontal and vertical coordinates

Greek symbols

α	thermal diffusivity of the fluid
β	coefficient of thermal expansion of the fluid
v	kinematic viscosity of the fluid
θ	dimensionless temperature $= (T - T_{\text{ref}})/\Delta T_i$
$\theta_{av} = \frac{T(t)_{av} - T_c}{\Delta T_i}$	instantaneous averaged non-dimensionalized temperature on left and right side walls
$\theta_b = \frac{T(t)_b - T_c}{\Delta T_i}$	instantaneous bulk (mass weighted average) non-dimensionalized temperature along a cross section on the center of the vent at $L/2$
ρ_0	reference density of the fluid
$\tau = t\alpha/L^2$	dimensionless time
$\Psi_b = V_{bmag}/V_{max}$	instantaneous mass weighted average velocity magnitude along a cross section located at the center of the gap i.e. at $L/2$. This velocity is normalized by the maximum velocity magnitude along the same location, where the maximum velocity magnitude is the highest velocity magnitude found on the domain at any time

stratification of fluid in the former case while the configuration is unstable for later. In spite of this fundamental difference, these studies offer a unique insight into flow mechanisms through apertures and different methodologies available to model them. Some of the prominent studies are reported here.

Prahl and Emmons [4] conducted an experimental and theoretical study of the fire induced flow through an opening in vertical partition. The experiments involved steady flows through a single opening with reduced scale kerosene/water analog. Inflow and outflow orifice coefficients were determined and found to be significantly different at low values of Reynolds number based on flow height but reached an asymptotic value of approximately 0.68 at large values of Reynolds number.

In the same year Leach and Thompson [5] carried out an experimental investigation of flows in horizontal circular tubes. For the whole range of $0.5 \leqslant L/D \leqslant 9.4$ and $3 \times 10^4 \leqslant Re \leqslant 1.5 \times 10^5$ investigated, they found that $C_D = 0.09$, a constant independent of L/D and Re_Δ. A large-scale experiment with carbon dioxide and water as working fluids was used to verify the above results for gases. They also investigated the forced flow rate requirements to prevent the counter current flow in the tube.

Brown [6] was first to study flow through square openings in horizontal partition with heavier fluid above the partition both analytically and experimentally. In his analysis, he assumed that all heat transfer is due to advection only and no mixing occurs within the vent. Assuming friction to be negligible, he invoked the Bernoulli's equation to predict that Nusselt number is proportional to product of square root of Grashof number and Prandtl number, the reference length being height of the vent. Brown and Salvason [7], did a similar analysis for a vent in a vertical partition to derive a theoretical relationship between Nu and Gr. An experimental study was reported by Epstein [8] of buoyancy driven exchange flow through small openings in horizontal partitions for the same geometric configuration as this study, Experimental apparatus consisted of two enclosures, one on top of the other, with brine and fresh water as working fluids. The study concentrated on finding the effect of height to diameter aspect ratio of the vent (L/D) on the dimensionless exchange flow rate as defined by Mercer and Thompson [9] in their study on inclined ducts. Four different flow regimes were identified as L/D was varied from 0.01 to 10. The first of these was named oscillatory exchange flow regime where plumes of fluids periodically broke through the opening. He used Taylor's wave theory to predict the motion of the interface and showed that the Froude number is a constant for this regime. Second flow regime was called the Bernoulli flow regime due to the fact that data showed same trends as predicted by Brown [6]. For this regime, he found that Froude number, $Q = 0.23(L/D)^{1/2}$ (length/width of the vent). For large L/D,

the flow rate was observed to be smaller than the other two regimes due to violent mixing within the vent. He used an analysis similar to that reported by Gardner [10] to provide correlations for his regime. An intermediate regime was also identified having combined characteristics of turbulent diffusion and Bernoulli flow.

Brine–Water analog was also studied experimentally by Conover and Kumar [11] and Conover et al. [12] studied experimentally the buoyant countercurrent exchange flow through a vented horizontal partition using a two-component laser Doppler velocimeter. Detailed measurements of velocity were made a small distance above a circular tube with an aspect ratio of 1. Even for this aspect ratio and a Reynolds number ranging between 2400 and 7700, the mixing in the vent was found to be turbulent and unsteady. He also found that the flow coefficient was nearly constant for a Reynolds number as low as 2400. This finding was in contrast with the work of [13] and [14] who showed that exchange flows reached self similarity only for Reynolds number greater than 10,000. Tan and Jaluria [15] and Jaluria et al. [16] studied cases where the vent flow was governed by both pressure and density differences across the vent.

Myrum [17] conducted heat transfer experiments using water in a top-vented enclosure heated by a disk on the enclosure floor. He observed four modes of flow, which were unstable and oscillated randomly from one to the next. More on this flow situation will be given in the results and discussion section.

A numerical study of unsteady buoyant flow through a horizontal vent placed slightly asymmetrically between two enclosed vents was performed by Singhal and Kumar [18]. A numerical investigation of countercurrent flow exchange through a vent in horizontal partition is performed by Spall and Anderson [19] for an infinitesimally thin partition. Harrison and Spall [20] studied numerically effects of axisymmetric partition thickness on counter current flow with water as the working fluid. They concluded that the flow exchange increases with increasing partition thickness over the range of $0.0376 <= L/D <= 0.3$, and decreases in the range of $0.3 <= L/D <= 1$. In their study the dimensions of the enclosure were fixed, while only the thickness of the partition is varied over a range of up to 1 only.

In all studies discussed above, only high *Ra* number ranges were investigated so that the effect of viscosity could be neglected and in general, flow coefficient or Froude number was considered a function of L/D only, independent of the driving potential. Also, the scaled brine – fresh water models used may not give comparable results to full scale air models due to large changes in the Prandtl number and the Schmidt number values at low *Ra*. Therefore, these models may not be applicable to the *Ra* of 10,000 investigated in this study.

An earlier study by the authors, Kumar et al. [21] identified the different flow regimes encountered for small to high Rayleigh number in a vented enclosure and discussed the physical mechanisms using the time trace of temperature and fluid flow results for a vent aspect ratio of one.

The objective of this study is to identify the effect of decreasing vent aspect ratio L/D to 0.5 and increasing it to 2 on the flow regimes found for the case of $L/D = 1$ for the same $Ra = 10{,}000$. The flow exchange between enclosures for $L/D = 0.5$, 1 and 2 is studied as well.

2. Governing equations and formulation

The time dependent governing equations for the laminar, two dimensional flow were derived from fundamental laws of conservation of mass, momentum and energy and are presented as follows:

$$\frac{\partial \rho}{\partial t} + \frac{\partial(\rho u)}{\partial x} + \frac{\partial(\rho v)}{\partial y} = 0 \tag{1}$$

$$\rho\left(\frac{\partial u}{\partial t} + u\frac{\partial u}{\partial x} + v\frac{\partial u}{\partial y}\right) = -\frac{\partial p}{\partial x} + \mu\left(\frac{\partial}{\partial x}\left(2\frac{\partial u}{\partial x} - \frac{2}{3}(\nabla\cdot\vec{v})\right) + \frac{\partial}{\partial y}\left(\frac{\partial u}{\partial y} + \frac{\partial v}{\partial x}\right)\right) \tag{2}$$

$$\rho\left(\frac{\partial v}{\partial t} + u\frac{\partial v}{\partial x} + v\frac{\partial v}{\partial y}\right) = -\frac{\partial p}{\partial y} + \mu\left(\frac{\partial}{\partial y}\left(2\frac{\partial v}{\partial y} - \frac{2}{3}(\nabla\cdot\vec{v})\right) + \frac{\partial}{\partial y}\left(\frac{\partial u}{\partial y} + \frac{\partial v}{\partial x}\right)\right) + \rho g \tag{3}$$

$$\frac{\partial T}{\partial t} + u\frac{\partial T}{\partial x} + v\frac{\partial T}{\partial y} = \alpha\left(\frac{\partial^2 T}{\partial x^2} + \frac{\partial^2 T}{\partial y^2}\right) + \frac{\beta T}{\rho C_p}\left(\frac{\partial p}{\partial t} + u\frac{\partial p}{\partial x} + v\frac{\partial p}{\partial y}\right) \tag{4}$$

L and α/L are used to normalize length and velocity respectively, α/L^2 to non-dimensionalize time and ΔT_1 to non-dimensionalize temperature.

The transient calculation approach considered in this study is not using the Boussinesq model that treats density as a constant value in all solved equations, except for the buoyancy term in the momentum equation. Instead the approach used here is that the initial density is computed from the initial pressure and temperature, so the initial mass is known. As the solution progresses over time, this mass will be properly conserved. When this approach is used the operating density, ρ_0 must appear in the body-force term in the momentum equation as $(\rho - \rho_0)g$. The

definition of the operating density ρ_0 is thus important for this buoyancy driven flow.

No slip conditions were used for velocity boundary conditions at all walls including the vent walls. Initially fluid is at rest everywhere in the domain, therefore velocity components were set equal to zero at non-dimentionalized time $\tau = 0$. All the walls were treated adiabatic and hence the normal gradients of temperature were set equal to zero at all fluid-wall interfaces. At $\tau = 0$, the lower chamber contains hot fluid with $\theta = 1$, while the upper chamber and the vent contain cold fluid with $\theta = 0$. The flow parameters of interest are *Ra* and *Pr*. *Pr* is maintained constant at 0.7. Referring to Fig. 1, the geometric parameters are vent aspect ratio, L/D, $H1/L$ and the enclosure aspect ratio, $H1/H2$. In this study these parameters are given in Table 1. Geometry for case 2 with $L/D = 0.5$ was achieved by scaling geometry of case 1 by a factor of 0.5 in the vertical (Y) direction. Similarly, geometry for case 3 with $L/D = 2$ was achieved by scaling geometry of case 1 by a factor of 2 in the vertical (Y) direction. For all three cases *Ra* was kept equal to 10,000.

Although the problem of natural convection in a horizontal cavity with bottom heating is highly three dimensional, it can be treated as two-dimensional problem for very long vents, which is the case considered in this paper.

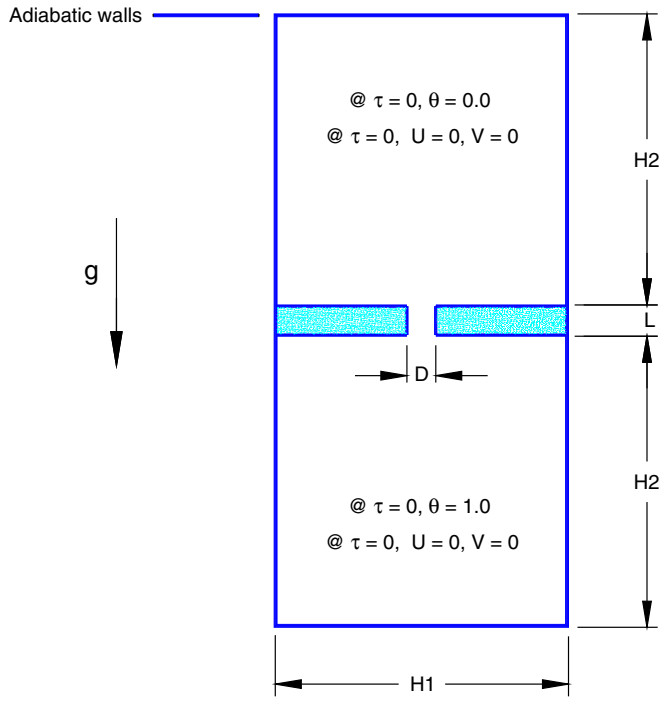

Fig. 1. Schematic diagram of the model.

Table 1
Investigated parameters

	L/D	$H1/L$	$H1/H2$
Case 1	1	10	1
Case 2	0.5	20	2
Case 3	2	5	0.5

3. Numerical procedure

Eqs. (1)–(4) are discretized over the computational domain using a control volume approach as documented in FLUENT documentations. Another approach for discretization can be found in Patankar [22]. The resulting algebraic equations for velocity components and temperature were solved using SIMPLE algorithm, which involves the use of pressure correction equations for enforcing mass conservation. FLUENT Code is used for this simulation. Segregated solver with first order implicit unsteady formulation is employed for this study. The air properties i.e. density, thermal conductivity, specific heat and dynamic viscosity are varied as a piecewise functions of temperature. By default, the solver will compute the operating density, ρ_0 that appears in the body-force term in the momentum equations as $(\rho - \rho_0)g$, by averaging over all cells. The discretization schemes used are second order for pressure, SIMPLE for pressure–velocity coupling and second order upwind for momentum and energy. The under-relaxation factor is 0.3 for pressure, 1 for density, body forces and energy and 0.7 for momentum. The code was tested by the authors in Ranganathan Kumar et al. [21] against certain benchmark solutions to validate the results. The predicted results were within 3% of these benchmark solutions.

Fig. 2 shows the numerical grid generated for this study using Gambit grid generator. Since FLUENT is an unstructured solver, it uses internal data structures to assign an order to the cells, faces, and grid points in a mesh and to maintain contact between adjacent cells. It does not, therefore, require i,j,k indexing to locate neighboring cells. This gives the flexibility to use the grid topology that is best for the problem, since the solver does not force an overall structure or topology on the grid. For the 2D problem considered here, quadrilateral cells are used to form multi-block structured mesh. More details on grid generation are provided in FLUENT documentation. A grid independent study is performed using three non-uniform grid dis-

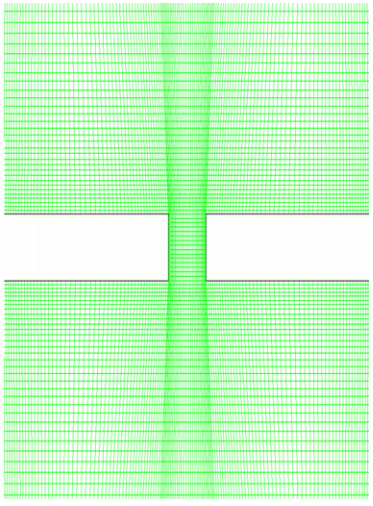

Fig. 2. Numerical grid.

tributions: coarse grid with 91×63 grid points used for every enclosure and 21×13 grid points used for the vent, medium grid with 133×91 grid points used for every enclosure and 31×19 grid points used for the vent and fine grid with 201×135 grid points used for every enclosure and 47×29 grid points used for the vent. The results for temperature and the two components of velocity at the center of the vent and at different locations inside the two enclosures for different Ra values were compared using all three grids. The maximum difference in temperature and velocities between coarse and medium grids found to be less than 1.5% when results from both grids are compared over the full time domain. The maximum difference between medium and fine grids found to be less than 0.2%. Finally, the non-uniform grid of 133×91 grid points was used for every enclosure and a grid of 31×19 grid points was selected for the vent with 7 grid points are clustered near every sidewall inside the boundary layer. One complete unsteady solution for one geometry and average Rayleigh number involved computation of up to 70,000 time step with approximately 30–40 iterations for every time step to have more confidence in results although a convergence usually is achieved after 10–15 iterations.

Convergence criteria were set to ensure converged results for continuity, X-velocity, Y-velocity and energy. A solution was assumed converged if the maximum scaled residuals of the continuity, X-velocity, Y-velocity and energy are 10^{-3}, 10^{-5}, 10^{-6} and 10^{-7}, respectively. The residual is scaled using a scaling factor representative of the flow rate of ϕ through the domain. This scaled residual is defined as

$$R^{\phi} = \frac{\sum_{\text{cells P}} |\sum_{\text{nb}} \alpha_{\text{nb}} \phi_{\text{nb}} + b - \alpha P \phi P|}{\sum_{\text{cells P}} |\alpha P \phi P|} \tag{5}$$

For the momentum equations the denominator term $\alpha p\ \phi p$ is replaced by $\alpha p\ vp$, where is the magnitude of the velocity at cell P.

The scaled residual is a more appropriate indicator of convergence. For the continuity equation, the solver's scaled residual is defined as

$$R^{\text{c}}_{\text{iteration}} N / R^{\text{c}}_{\text{iteration}} 5 \tag{6}$$

The denominator is the largest absolute value of the continuity residual in the first five iterations.

For the enclosure under consideration, a fixed time stepping method is used for time marching scheme. The time step used was based on estimating the time constant as Bejan [23]:

$$t_{\text{c}} = \frac{L}{U} \approx \frac{L^2}{\alpha} (PrRa)^{-1/2} = \frac{L}{\sqrt{g\beta \Delta T_{\text{i}} L}}$$

where L and U are the length and the velocity scales, respectively.

Then the time step is determined such that $\Delta t = \frac{t_c}{20}$. Note that this time step value used in this study is five times less than the recommended time step in open literature to ensure time convergence. After oscillations with a typical frequency have decayed, the solution reaches steady state.

The time step independence was tested prior to obtaining solution for the desired problem. The time independent study is established by tracking the changes in temperature and the two components of velocity at a point located at the center of the vent by increasing and decreasing the time step for all cases of Ra studied. Decreasing the time step from $\Delta t = \frac{t_c}{20}$ to $\Delta t = \frac{t_c}{25}$ resulted in less than 0.05% difference in temperature and velocities when results from both time steps are compared over the full time domain. Increasing the time step from $\Delta t = \frac{t_c}{20}$ to $\Delta t = \frac{t_c}{15}$ resulted in less than 0.1% difference in temperature and velocities when results from both time steps are compared over the full time domain. Based on this, the time step used for all simulations is $\Delta t = \frac{t_c}{20}$. Fig. 3 shows sample convergence plots of the scaled residual for $Ra = 10{,}000$ at different time steps.

4. Quantities of interest

The Rayleigh number was defined as $Ra = (g\beta \Delta T_{\text{i}} L^3)/v\alpha$, where ΔT_{i}, is the initial temperature difference between the two enclosures (i.e. at $\tau = 0$). As the interaction between the fluids in the two enclosures proceeds with time, the effective driving potential is the temperature difference across the vent and not ΔT_{i}. Magnitude of the temperature difference across the vent decreases with time. Therefore, new quantities need to be defined which would reflect this change in driving potential with time. To this end, we define the following quantities:

(1) Instantaneous averaged non-dimensionalized temperature (θ_{av}) on left and right side walls of the vent defined as: $\theta_{\text{av}} = \frac{T(t)_{\text{av}} - T_{\text{c}}}{\Delta T_{\text{i}}}$. Thus ($\theta_{\text{av}}$) will vary from 0 to 1.
(2) Instantaneous bulk (mass weighted average) non-dimensionalized temperature (θ_{b}) along a cross section on the center of the vent at $L/2$ defined as: $\theta_{\text{b}} = \frac{T(t)_{\text{b}} - T_{\text{c}}}{\Delta T_{\text{i}}}$. Thus ($\theta_{\text{b}}$) will vary from 0.0 to 1.0.
(3) Instantaneous mass weighted average velocity magnitude (Ψ_{b}) along a cross section located at the center of the gap i.e. at $L/2$. This velocity is normalized by the maximum velocity magnitude along the same location ($\Psi_{\text{b}} = V_{\text{bmag}}/V_{\text{max}}$), where the maximum velocity magnitude is the highest velocity magnitude found on the domain at any time. Thus (Ψ_{b}) will vary from 0.0 to 1.0. All quantities described above are then calculated at every time step through out the simulation.

5. Results and discussion

The interaction between the two enclosures takes place through the vent and the flow patterns within the vent determine the mode of heat transfer and the rate of heat

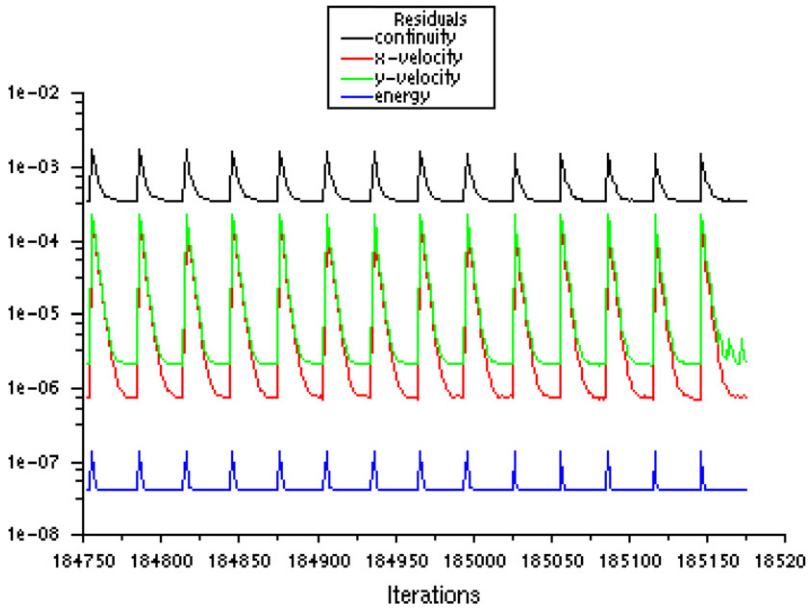

Fig. 3. Scaled residuals for $Ra = 10{,}000$, time = 4616 s and $L/D = 1$.

and mass transfer across it. These flow patterns in the vent are dependent on the vent geometry, the magnitude of the buoyancy force which drives the flow across it and to a great extent the flow patterns in enclosures themselves. The last category mentioned above makes the flow configuration difficult to analyze. However, from the results presented, an attempt has been made to explain the localized phenomena. Based on the mode of heat transfer and the associated flow characteristics, three categories have been identified by the authors in previous work [21] for $L/D = 1$. These are the conduction regime, the countercurrent regime and the oscillatory regime. The Rayleigh number as explained below largely governs these regimes. In this study the effect of vent aspect ratio is studied for fixed initial $Ra = 10{,}000$, which is found to be an oscillatory flow regime for the case of $L/D = 1$.

5.1. Baseline case of L/D = 1

Fig. 4 shows overall velocity field and Fig. 5 gives a magnified view of the velocity field in the vent for the case of $L/D = 1$. At $\tau = 1.35$ the oscillatory flow regime is dominating, which is characterized by sudden bursts of both upflow and downflow. At $\tau = 2.31$ the flow still oscillatory but with higher frequency as shown in Fig. 6. At $\tau = 14.37$ the flow regime is starting to change to counter current. At this time the flow in upper and lower enclosures is not symmetrical yet. The symmetry is achieved around $\tau = 42$ where the flow regime becomes conduction one. The conduction flow regime continues until the flow comes to complete rest at high τ values.

The average temperature of the right and left walls of the vent and the mass weighted average temperature in the vent are shown by Figs. 7–9, respectively. The difference in temperature between left and right walls at $L/D = 1$ is obvious and is a result of the unsymmetrical flow patterns inside the vent, especially for the oscillatory flow regime.

5.2. Case of L/D = 0.5

Figs. 10 and 11 show overall velocity field and magnified view of the velocity vectors inside the vent for $L/D = 0.5$. At low $\tau = 0.8$ the heavier and slower flow from the top enclosure tends to penetrate through the vent towards the lower enclosure. The resistance from the lighter hotter fluid in the lower enclosure is increasing until finally it penetrates to the upper enclosure at $\tau = 4.3$. At this time level the highest velocities are found in upper enclosure. At $\tau = 10.73$ the fluid of the upper enclosure is trying to resist to penetrate to the lower enclosure where at this time level the highest velocities are found in lower enclosure. It is found that the flow at this $L/D = 0.5$ does not have that signs of oscillatory flow regime observed for $L/D = 1$ where a large vortex formed in the vent. Instead the flow is oscillating with higher frequency between the two enclosures until it reaches the conducting flow regime at high time levels of τ more than 50. The full symmetry of the flow in the upper and lower enclosures is reached at time levels of around $\tau = 63$.

5.3. Case of L/D = 2

Figs. 12 and 13 show overall velocity field and magnified view of the velocity vectors inside the vent for $L/D = 2$. The flow for this case is solely conducting at all time levels. At low $\tau = 0.135$ the heavier slower flow from the top enclosure tends to penetrate through the vent towards the lower enclosure but the high resistance from the lighter hooter fluid in the lower enclosure prevents its penetration.

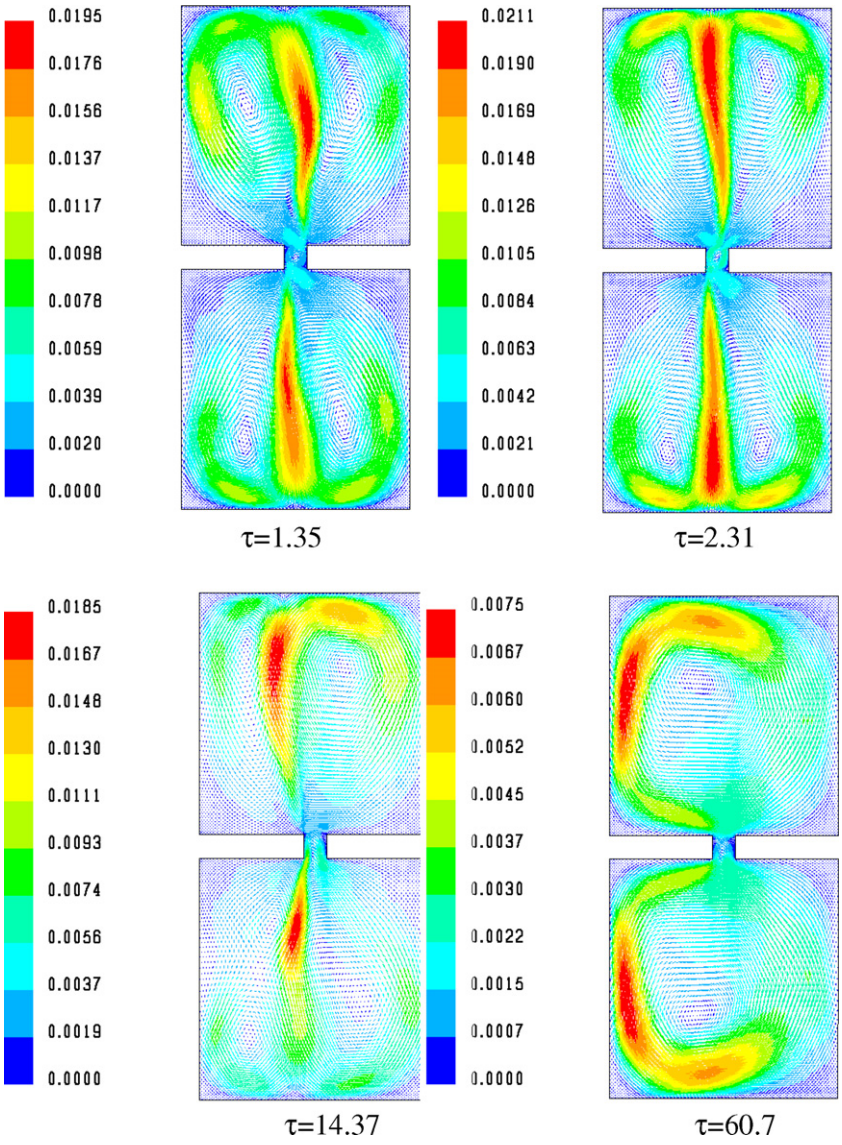

Fig. 4. Overall velocity field for $L/D = 1$ (colored by velocity magnitude; m/s).

The first mode of symmetry of the flow in the two enclosures is reached at low $\tau = 0.5$. This symmetry is characterized by large vortex, which occupies the whole enclosure. At $\tau = 0.2$ (not shown) a second vortex is starting to form on the upper half of the upper enclosures as a results of the motion of the flow, which is coming back from the vent region. This flow, being not strong enough to travel all the way to the upper wall of the upper enclosure, is turning back at location above the center of the enclosure causing two counter current vortices of different size and velocity. At this time level no second vortex is found in the lower enclosure. This second vortex in lower enclosure is starting to appear only at $\tau = 4$ (not shown) and is completely shaped at $\tau = 10$ (not shown). The flow in both enclosures at all higher time levels is characterized by those four vortices while the flow exchange in the vent is solely by conduction.

This singular phenomenon of no flow at low *Ra* numbers is analogous to Benard convection problem. At $\tau = 0$ fluid is at rest everywhere and the vent marks the region of separation of large bodies of hot and cold fluid. With respect to the vent, the denser fluid is at the top with a natural tendency to exchange its place with the lighter fluid at the bottom of the vent. However, this exchange is inhibited by its own viscosity and for the flow to issue; the adverse temperature gradient must exceed a certain value. The onset of instability beyond a critical value of the Rayleigh number has been thoroughly analyzed using techniques such as linear stability theory and power integral method. Chandrasekhar [24] has presented a comprehensive treatment of the linear stability theory where he has shown mathematically the thermodynamic significance of Ra_{critical}. In his words: "Instability occurs at the minimum temperature gradient at which a balance can be steadily

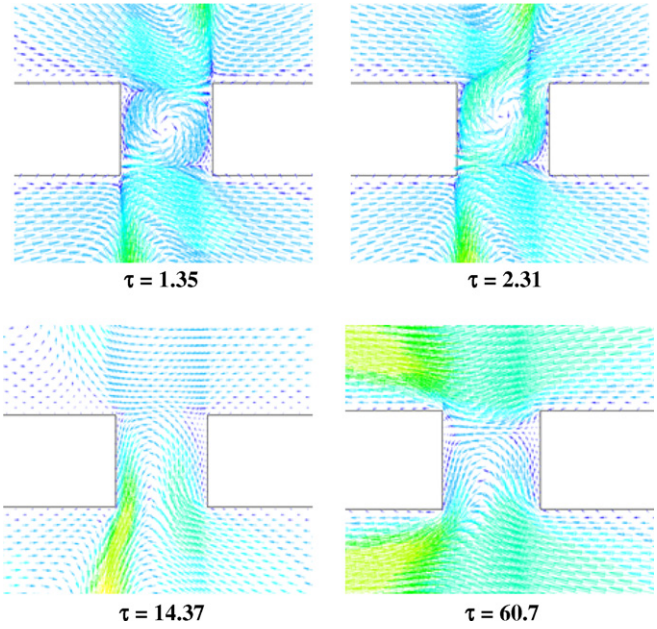

Fig. 5. Magnified view of the velocity field in the vent for $L/D = 1$.

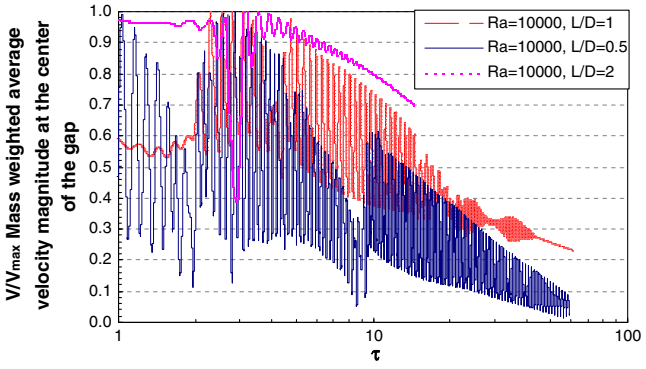

Fig. 6. Time trace of instantaneous mass weighted average velocity magnitude (Ψ_b).

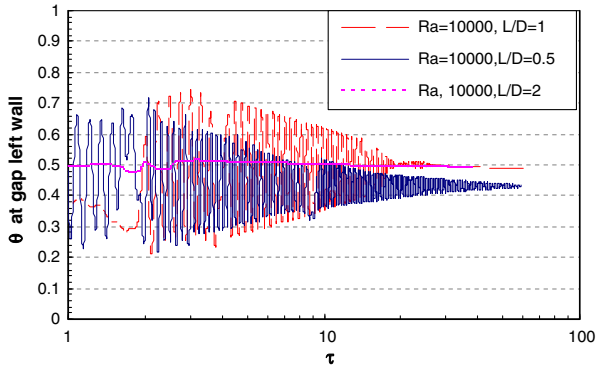

Fig. 7. Time trace of θ_{av} on the right wall of the vent.

maintained between the kinetic energy dissipated by viscosity and the internal energy released by the buoyancy force". $Ra_{critical}$ corresponds to the above-mentioned minimum temperature gradient in conjunction with the dynamical conditions at the two bounding planes. For the case of

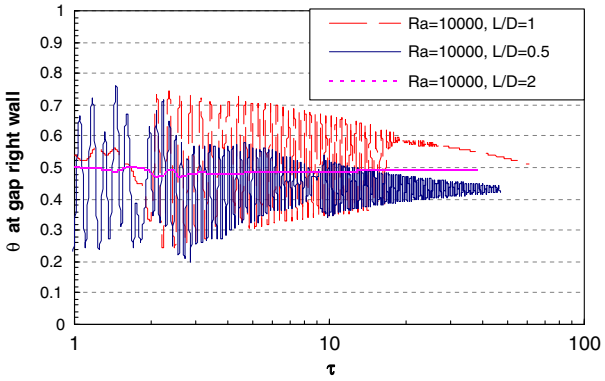

Fig. 8. Time trace of θ_{av} on the left wall of the vent.

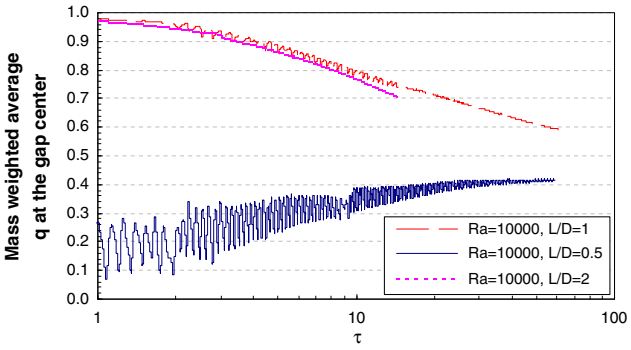

Fig. 9. Time trace of instantaneous bulk (mass weighted average) non-dimensionalized temperature (θ_b).

rigid constant temperature surfaces, $Ra_{critical}$ has been calculated to be 1708, for one rigid and one free surface it is 1100 and for both free surfaces $Ra_{critical}$ is found to be 658. The same line of reasoning can be applied to the flow in the vent. This is justified if one takes a closer look at Figs. 5, 11 and 13, which show a magnified view of velocity vectors in the vent. The following observation can be made. The magnitude of velocity in the vent for $L/D = 2$ is extremely small as compared to those in the enclosures. In the middle of the vent, velocities are negligible suggesting that the fluid movement at the top and bottom edges of the vent is due to bulk fluid motion in the enclosures. Two planes of symmetry exist dividing the vent into four similar parts. Several complications arise in this problem, which makes stability analysis difficult. One is the effect of side walls and the other is the influence of bulk fluid motion in upper and lower chambers, the later being more complex than the former. To date, several researchers have addressed the issue of the effect of side walls on $Ra_{critical}$. First complete analysis was given by Yih [25] for the stability of a viscous fluid between insulated vertical plates. Davis [26] was the first to consider the fully confined fluid. He used the Galerkin method for his analysis. Later Catton [27] improved on his results and produced a chart for $Ra_{critical}$ as a function of H1 and H2 as parameters, where H1 and H2 are spanwise dimension and depth, respectively. Both studies considered the side walls to be perfectly conducting walls.

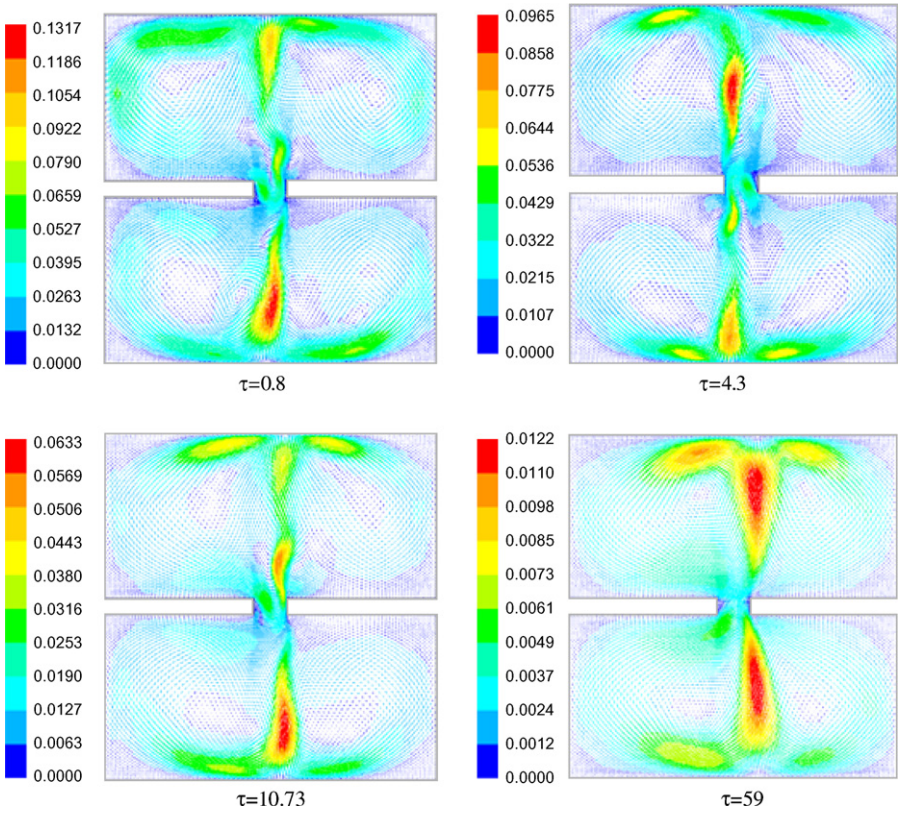

Fig. 10. Overall velocity field for $L/D = 0.5$ (colored by velocity magnitude; m/s).

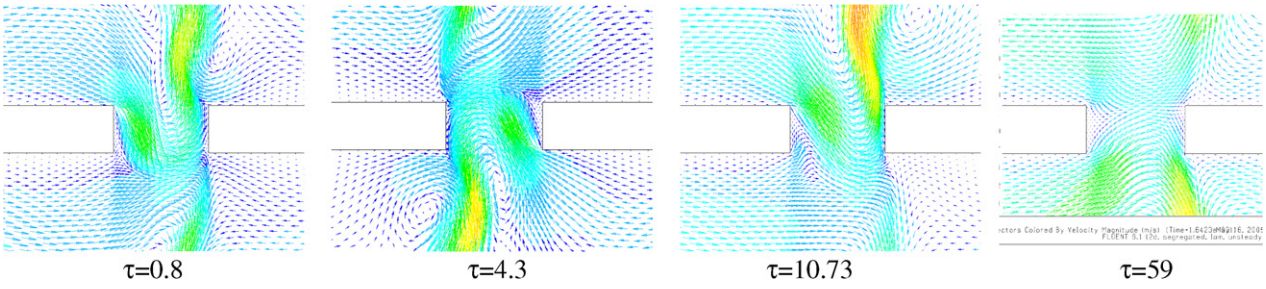

Fig. 11. Magnified view of the velocity field in the vent for $L/D = 0.5$.

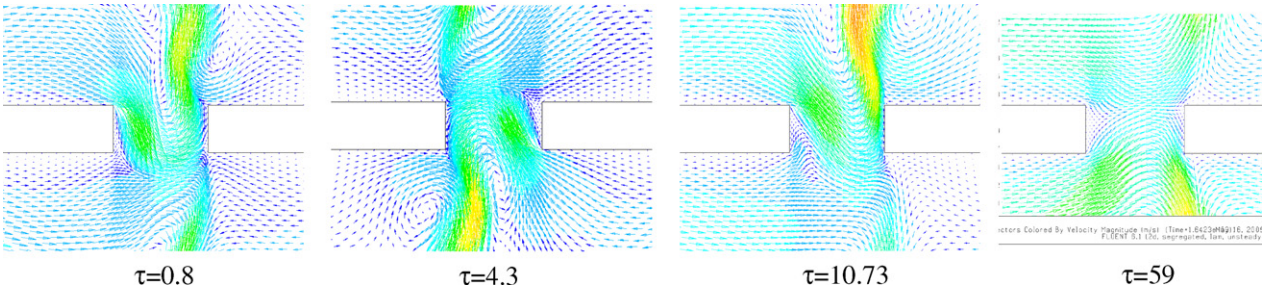

Fig. 12. Overall velocity field for $L/D = 2$ (colored by velocity magnitude; m/s).

Later, Catton and Edwards [28] performed an experimental study on the effects of side wall on natural convection. They were able to obtain Ra_{critical}. as a function of height to width ratio for insulating as well as conducting lateral walls. For an aspect ratio of 1.0 and insulating lateral walls, they reported that Ra_{critical} was in the range of $1 \times$

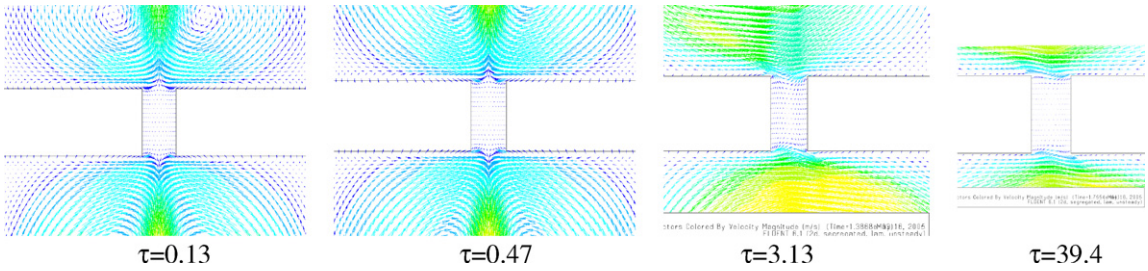

Fig. 13. Magnified view of the velocity field in the vent for $L/D = 2$.

10^4 and 2×10^4. They also developed a heat transfer correlation.

On the second issue mentioned above regarding the influence of bulk fluid motion in enclosures on the vent no prior works exists. Figs. 7 and 8 give the change in θ_{av} on right and left walls of the vent, respectively, as a function of time. Instantaneous bulk (mass weighted average) non-dimensionalized temperature (θ_b) along a cross section on the center of the vent at $L/2$ is given by Fig. 9 and the instantaneous mass weighted average velocity magnitude (Ψ_b) is shown by Fig. 6.

For very small values of τ, a sharp gradient appears in (Ψ_b) because of the initial conditions imposed in the enclosures. However, the flow adjusts itself quickly to decrease this gradient as (θ_b) steadily decreases with time. Since all the heat transfer is by conduction only, the average wall temperature θ_{av} is having a constant value of about 0.5 for all values of τ.

For $L/D = 1$ case, the countercurrent regime is characterized by a down flow along approximately one half of the vent and upflow along the rest to satisfy continuity. One essential difference in the flow patterns between conduction and countercurrent regimes is that the cells in the top chamber for counter current regime become asymmetric at early non-dimensional times. This asymmetry arises during the onset of the countercurrent flow at the vent. A closer look at the vent clearly shows the upflow on the right side and downflow on the left side of the vent. With time, the flow gradually reverts itself to the conduction regime with one large cell in each chamber. As Rayleigh number is increased in this flow regime, the flow patterns present the most interesting phenomenon. In Fig. 10 at $\tau = 2.31$, the flow patterns are strictly countercurrent in the vent, however, at $\tau = 8$ (not shown), the flow everywhere in the enclosure slows down. This is evident from the magnified view of the vent in Fig. 11. Following this deceleration, a flow reversal occurs at the vent at $\tau = 11$ and lasts as seen at $\tau = 14.37$ up to $\tau = 19$ (not shown) and the flow accelerates again as evident by the magnitude of velocity vectors. This is the only flow reversal that occurs in this flow regime. Such a phenomenon has also seen by Myrum [17]. He conducted an experimental study to find the effect of vent size and Ra on natural convection heat transfer from a heated disk. This disk was located at the bottom of a top vented enclosure. During the experiments, he also studied the flow patterns in the vent and reported four basic modes. In mode I, flow exited the vent along its axis and entered around its circular perimeter. In mode II, regions of outflow and inflow formed concentric rings within the vent. In mode III, inflow occurred through one half of the vent along the perimeter and corresponding outflow through the rest. A non-periodic shift in sides of inflow and outflow was also observed as seen in the current flow situation.

Although a direct comparison cannot be made of the current study and Myrum's Myrum [17], the time history of heat transfer along with numerical flow visualization reveal mode III. At the time of this change in direction near $\tau = 8$ as discussed above, the exchange flow rate decreases drastically with corresponding decrease in heat transfer across the vent as seen in Figs. 8 and 9. This change, therefore, appears in θ_b and Ψ_b time history as a sudden decrease. A sharp decrease and increase in the rate of change of instantaneous θ_{av} on the right and left walls of the vent respectively occur as shown by Figs. 6 and 7 due to the flow reversal. As soon as the change in sides is complete the average and bulk temperatures and velocities resume at almost the same values as before the change. At large values of τ flow in the vent gradually dies out due to lack of driving potential, namely the bulk-mean temperature difference between the two enclosures. As this happens, the plumes are no longer strong enough to sustain two cells on either side and gradually, the two cells merge to form a single cell. Since at this point of time there is no flow across the vent, the heat transfer is by conduction only.

This oscillatory regime is characterized by sudden bursts of both upflow and downflow for case 1 of $L/D = 1$. This shows up as a periodic-like response in θ_{av}, θ_b and Ψ_b time history for $L/D = 0.5$ and 1 only as shown in Figs. 6–9. This type of flow originates at nearly $Ra = 3600$ for case 1 with $L/D = 1$. For case 2 with $L/D = 0.5$ similar sudden bursts of upflow and downflow seen with $L/D = 1$ can be observed clearly. The periodic like response in $\theta_{av}$is shifted with higher frequency and less magnitude as a result of the higher frequency and larger magnitude of Ψ_b. The mass weighted average temperature in the gap, θ_b is no longer originating at 1 with low frequency as with the case of $L/D = 1$, instead θ_b is characterized by high frequency bursts, which can be explained as the result of the initial high temperature difference between the two enclosures used to maintain $Ra = 10{,}000$.

For case 3 with $L/D = 2$, the flow regime is no longer oscillatory. A very similar patterns to those observed for conduction regime when $L/D = 1$ can be seen clearly for $L/D = 2$. In the conduction regime, the buoyancy forces are not strong enough to overcome the viscous forces in the vent where the vertical walls of the vent are closer to each other as compared to the enclosure's vertical walls. Consequently, there is no bulk fluid motion within the vent, as shown by Fig. 13, and all the heat transfer is solely by conduction. In this regime, the vent acts like a heater plate for the upper chamber, which is filled with colder fluid and as a cold plate for lower chamber, which is filled with warmer fluid. Thus, in the enclosures bulk fluid motion ensues immediately after the initial establishment of temperature gradient in vent. A plume rises steadily into the upper chamber forcing the colder fluid to move along the side walls to replace the rising fluid forming two cells of equal strength on either side of it. For some time, the cells stay symmetric in each chamber. Then the cells in the upper chamber become asymmetric before splitting into two cells. There is a time delay before the lower chamber behaves exactly like the upper one exhibiting two cells. At large τ, the fluid in the chambers has accelerated enough to drive the fluid in vent by entrainment/shear.

In the oscillatory flow regime, unlike the other two regimes (conduction and counter current), the flow in the bottom chamber reaches a unicellular pattern earlier than the top enclosure. A close look at the flow patterns within the vent, as given in Fig. 13, reveals that the cell that develops in the vent persists for a longer period before they undergo a flow reversal as seen before. Temperature and velocity plots for $Ra = 10{,}000$ at different times (Figs. 6–9) give a unique perspective of occurrences in the vent. Temperature and velocity inversions occur at different times corroborating the fact that the flow oscillates with a well-defined frequency in the entire domain.

It is suspected that these bursts are periodic in nature and the frequency of bursts is a function of driving potential. Time traces of Ψ_b and θ_{av}, θ_b for $Ra = 10{,}000$ (Figs. 6–9) suggest that there are varying amplitude oscillations in a narrow frequency range that eventually die out and essentially reproduce the flow behavior quantified in the countercurrent and conduction flow regimes at large non-dimensional time. The Nusselt number trace was observed by Mitchell and Quinn [29] in a confined layer heated from below. They found that as the plate temperature was increased, the fluid oscillated in a narrow frequency band. They also noted that the oscillations were stable over a large Rayleigh number range. Once again, a direct comparison of our results with those of Mitchell and Quinn [29] cannot be made since their mean flow was steady.

6. Conclusion

A numerical study of unsteady, laminar, buoyant flow through a horizontal rectangular vent between two large enclosures was performed for three cases of $L/D = 0.5$, 1 and 2. Based on the flow patterns in the vent and the corresponding modes of heat transfer through it, the three flow regimes identified for the case of $L/D = 1$: the conduction regime, the countercurrent flow regime and the oscillatory flow regime are no longer exists for the case of $L/D = 2$. Instead only the conduction flow regime is observed, where there is no flow across the vent, the viscous forces being as large as the buoyancy forces.

Temperature and velocity results associated with bursts in the oscillatory flow regime for $L/D = 0.5$ and 1, display interesting characteristics of increasing amplitudes but nearly the same frequency. Such oscillations were also documented by Mitchell and Quinn [29] for a steady mean flow convection experiment in an unvented enclosure.

Decreasing partition thickness from $L/D = 1$ to 0.5 increases the flow exchange between the upper and lower enclosures with increasing frequency of the oscillatory flow pattern. Increasing partition thickness from $L/D = 1$ to 2 decreases the flow exchange between the two enclosures and flow regime becomes conduction with low frequency.

References

[1] Y. Jaluria, Natural Convection Heat and Mass Transfer, Pergamon Press, UK, 1980.
[2] S. Dhimdi, P. Vandevelde, Electrical analogy in heat and smoke evacuation, Int. J. Architect. Sc. 2 (2001) 1–6.
[3] A. Kashef, N. Bénichou, G.D. Lougheed, Numerical modelling of movement and behaviour of smoke produced from fires in the Ville-Marie and L.-H.-La Fontaine tunnels: literature review, Research Report, Institute for Research in Construction, National Research Council Canada, September 1, vol. 141, 2003, p. 66 (IRC-RR-141).
[4] J. Prahl, H.W. Emmons, Fire induced flow through an opening, Combust. Flame 25 (1975) 369–385.
[5] S. Leach, H. Thompson, An investigation of some aspects of flow into gas cooled nuclear reactors following and accidental depressurization, J. Br. Nucl. Energy Soc. 14 (1975) 243–250.
[6] W. Brown, Natural convection through rectangular openings in partitions – 2: Vertical partitions, Int. J. Heat Mass Transfer 5 (1962) 295–299.
[7] W. Brown, K. Salvason, Natural convection through rectangular openings in partitions – 1: Vertical partitions, Int. J. Heat Mass Transfer 5 (1962) 859–868.
[8] M. Epstein, Buoyancy driven exchange flow through small openings in a horizontal partitions, J. Heat Transfer 110 (1988) 885–893.
[9] A. Mercer, H. Thompson, An experimental investigation of some further aspects of the buoyancy-driven exchange flow between carbon dioxide and air following a depressurization accident in a magnox reactor, Part 1: The exchange flow in inclined ducts, J. Br. Nucl. Energy Soc. 14 (1975) 327–334.
[10] G. Gardner, Motion of miscible and immiscible fluids in closed horizontal and vertical ducts, Int. J. Multiphase Flow 3 (1977) 305–318.
[11] T.A. Conover, R. Kumar, LDV study of buoyant exchange flow through a vertical tube, in: Proceedings of the 5th International Conference on Laser Anemometry, Advances and Applications, Veldohoven, Netherlands, 1993.
[12] T.A. Conover, R. Kumar, J.S. Kapat, Buoyant pulsating exchange flow through a vent, J. Heat Transfer 117 (1995) 641–648.
[13] K. Steckler, H. Baum, J. Quintiere, in: Twenty first Symposium (International) on Combustion, The Combustion Institute, 1986.
[14] K. Steckler, H. Baum, J. Quintiere, Fire induced flows through room openings-flow coefficients, in: Twentieth Symposium (International) on Combustion, The Combustion Institute, 1984.

[15] Q. Tan, Y. Jaluria, Flow through a horizontal vent in an enclosure fire, Fire Combust. Syst., ASME HTD 199 (1992) 115–122.
[16] Y. Jaluria, S.H.-K. Lee, G.P. Mercier, Q. Tan, Visualization of transport across a horizontal vent due to density and pressure difference, Visualizat Heat Transfer Processes, ASME HTD, 1993.
[17] T. Myrum, Natural convection from a heat source in a top-vented enclosure, J. Heat Transfer 112 (1990) 632–639.
[18] M. Singhal, R. Kumar, Unsteady buoyant exchange flow through a horizontal partition, J. Heat Transfer 117 (1995) 515–520.
[19] R.E. Spall, E.A. Anderson, A numerical study of buoyant, pulsating exchange flows through a vent in a thin horizontal partition, Numer. Heat Transfer Part A 36 (1999) 263–272.
[20] R.P. Harrison, R.E. Spall, The effect of partition thickness on buoyant exchange flow through a horizontal opening, J. Numer. Heat Transfer (2003) 44.
[21] Ranganathan Kumar, Ahmad Sleiti, J. Kapat, Unsteady laminar buoyant flow through rectangular vents in large enclosures, AIAA J. Theromphys. Heat Transfer 20 (2006).
[22] S.V. Patankar, Numerical Heat Transfer and Fluid Flow, Hemisphere Publ. Corp., 1980.
[23] A. Bejan, Convection Heat Transfer, John Wiley and Sons, New York, 1984.
[24] S. Chandrasekhar, Hydrodynamic and Hydromagnetic Stability, Oxford Clarendon Press, London, 1961.
[25] C.S. Yih, Thermal instability of viscous fluids, Quart. Appl. Math. 17 (1959) 25.
[26] G. Davis, G. De Vahl, Natural convection of air in a square cavity: a bench mark numerical solution, Int. J. Numer. Meth. Fluids 3 (1983) 249–264.
[27] I. Catton, Convection in closed rectangular region: the onset of motion, J. Heat Transfer (1970) 186–188.
[28] I. Catton, D.K. Edwards, Effect of side walls on natural convection between horizontal plates heated from below, J. Heat Transfer (1967) 295–299.
[29] W.T. Mitchell, J.A. Quinn, Thermal convection in a completely confined fluid layer, AIChE J. 12 (1966) 1116–1124.